Experimental Investigation of Topology-Optimized Reinforced Concrete Beams with Varying Volume Fractions

By

Yan Liu

B.Sc. Civil Engineering
Johns Hopkins University, Baltimore, 2018

SUBMITTED TO THE DEPARTMENT OF CIVIL AND ENVIRONMENTAL ENGINEERING IN PARTIAL FULFILLMENT OF THE REQUIREMENTS FOR THE DEGREE OF

MASTER OF ENGINEERING IN CIVIL AND ENVIRONMENTAL ENGINEERING
AT THE
MASSACHUSETTS INSTITUTE OF TECHNOLOGY

June 2019

Signature redacted
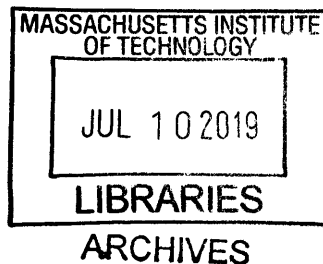
Signature of Author: _____
Department of Civil and Environmental Engineering
May 10th, 2019

Signature redacted

Certified by: _____
Josephine Voigt Carstensen
Lecturer of Architecture and Civil and Environmental Engineering
Thesis Supervisor

Signature redacted

Accepted by: _____
Heidi Nepf
Professor of Civil and Environmental Engineering
Chair, Graduate Program Committee

Experimental Investigation of Topology-Optimized Reinforced Concrete Beams with Varying Volume Fractions

By

Yan Liu

Abstract

Researchers have developed algorithms for topology optimization of concrete and reinforced concrete designs. However, concrete is a complex composite material and there is still a lack of validation of fabricated topology-optimized designs of concrete structures. It hinders the progress of incorporating topology-optimized structural components in the civil engineering industry. This work aims to address the issue stated above by experimentally evaluating deep reinforced concrete beams with strut-and-tie models (STMs) designed with the Hybrid Truss-Continuum Topology Optimization Algorithm [5]. The algorithm is chosen to alleviate the need for post-processing as it incorporates the discrete nature of the steel reinforcement in the design problem which allows continuous force flow within the concrete phase of the design. The hybridity, therefore, originates from a truss element ground structure design in the density-based continuum topology optimization framework. The resultant optimized truss elements represent the tensile load path whereas the optimized continuum structure indicates the compressive load path.

When using STM to design reinforced concrete beams, there will be underutilized areas within the concrete phase where minimal force is predicted to be present. In this work, we experimentally investigate the consequences of removing material in these regions. The used algorithm [5] is adjusted to enable control of the volume fraction of both the reinforcing and the concrete phase. A preliminary relationship between the reduction in strength of the reinforced concrete beams and the extracted volume of the underutilized areas is explored. The design domain is a 2D prismatic deep reinforced concrete beam with dimensions 3 feet by 9 inches by 2 inches. The tested beams are simply supported with a single point load at mid-span. Using the same steel volume, concrete volume fractions of 75%, 85%, 90%, 95%, and 100% are presented and experimentally tested.

Thesis Supervisor: Josephine V. Carstensen
Title: Lecturer of Civil and Environmental Engineering

Acknowledgement

My journey at MIT was made possible by the generosity and support of my parents. While one can quantify the amount of financial support, I certainly cannot put a value on how much my parents have provided me. Although they are on the other side of the earth, their care has always been around me. Also, the encouragement and hope provided by my girlfriend, who is also not present with me, have accompanied me throughout my time at MIT. Being cared and loved by someone is something very solid. This love always fueled me to push harder and investigate more.

Not a single part of this thesis is possible without the care of professor Josephine Carstensen. She made me realize that topology optimization is not a convoluted enigma, but something very tangible, powerful, and practical. I thank her for her wealth of knowledge, the warmth and joy brought by her conversation, her patience and especially her care. It is because she cares that she pushed me to the best of my ability. She makes me feel like my work is worth something, something more than a degree requirement. I would also like to thank Jackson Jewett, a former MEng, for his help. He passed down he knowledge from last year which prevented me from making a lot of mistakes that could seriously hinder the progress.

During the construction process, I would like to thank Steve for his countless hours of help and his expertise in experiments. I would like to thank Moh for his expertise in design and casting of concrete structures. I would like to thank the architectural shop at MIT, especially the TAs, for their help in manufacturing the crucial components of this research. I would like to thank all who offered help and support in this process and in the entirety of my thesis.

At the start of the semester when professor Mueller asked us what our anticipations were for this program, I replied that I was excited to share the learning experience with my peers. At nearly the end of the school year now, I must admit that I have had a journey of a life time with them. Tim, Andrew, Julien, Karly, Charlotte, Enrique, Judy, Abigail, and Nifemi, you guys make the MEng room feel like a place to which I belong. Thank you all for this unbelievable journey. I wish you all a bright start of your next stage of life and an even brighter future.

Table of Content

List of Figures

List of Tables

1. Introduction

First became prevalent in ancient Rome, concrete is still one of the most important building materials that construct our cities today [1]. The introduction of steel reinforcement in the weak tension regions within concrete significantly increases its capacity. On the one hand, concrete is a highly malleable material and, thus, enables a myriad of structural forms. On the other hand, its non-uniform nature still poses challenges during the design and construction phase [2].

Topology optimization is a design algorithm that optimally distributes material in a design domain given the prescribed loading and support conditions [3]. Topology optimization has fostered possibilities of developing new designs with exciting properties. It is capable of producing high performance structural solutions comparing to conventional designs. Two types of optimization formulation, Truss Topology Optimization and Continuum Topology Optimization, are frequently investigated by researchers. While we are witnessing an increasing use of topology optimization in the automotive and aerospace industries, the lack of fabrication techniques and validated algorithms significantly hinders its development in civil structures.

Researchers have proposed topology optimization algorithms that try to capture the complex nature of the concrete, while others focus on high-performance truss optimization. This paper is based on the algorithm developed by Gaynor et al. [5]. Traditionally, designing of steel reinforcement is a separate process where the reinforcement is typically sized based on axial forces, assuming the concrete phase has cracked to its neutral axis [4]. The topology optimization algorithm proposed by Gaynor et al. [5] enables us to link the concrete phase with its reinforcement and design them simultaneously. The algorithm proposes using the strut-and-tie model (STMs) with the hybrid truss-continuum optimization. The STM uses a statically determinate truss to approximate the non-linear behavior of a deep reinforced concrete beam to produce a safe and sound design.

Using STM to analyze and design reinforced concrete beams will result in under-utilized areas within the concrete phase. This paper aims to experimentally investigate the consequences of removing material from such regions. Firstly, this paper will introduce the modifications made to Gaynor's algorithm as well as the manufacturing process of the beams. Secondly, the experimentally tested capacity of the optimized reinforced concrete beams with varying volume fractions will be presented and the results will be discussed. A relationship

between the reduction in strength and the amount of material removed is the target of this research.

2. Literature Review

When it comes to real-world civil structures, examples of optimization are scarce because of the lack of manufacturing techniques and the high cost of fabrication. Although bounded by such constraints, structural engineers never abandon the goal of optimizing the performance of a building.

Designed by the Japanese architect Arata Isozaki, the façade of the Qatar National Convention Center, displayed in Fig.2-1, resembles a tree that reaches to support the upper canopy. The branch-like mega-columns are inspired by the results of Bi-Directional Evolutional Structural Optimization [10]. The design also symbolizes the essence of the desert and the thirty for knowledge, which is made possible with the optimization algorithm [11].
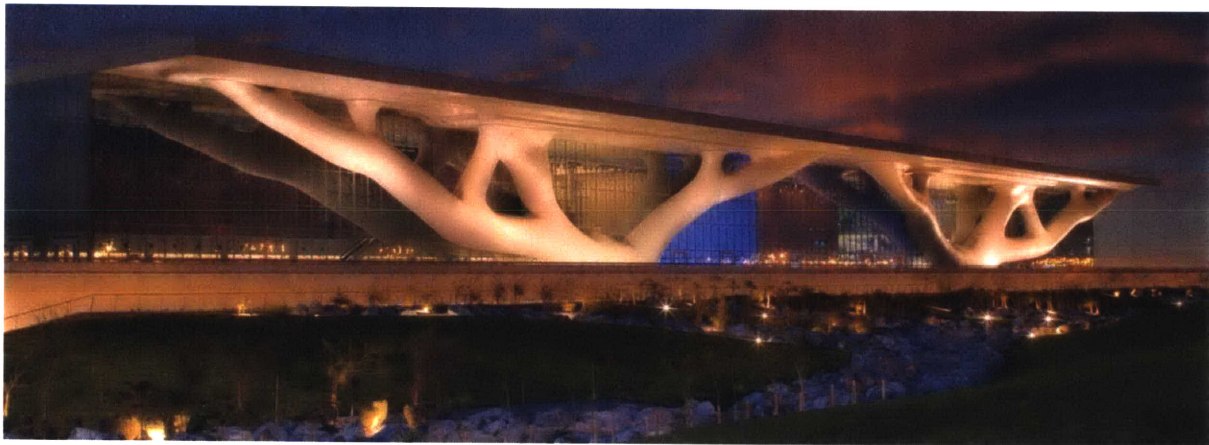
Fig.2-1 Façade of the Qatar National Convention Center

Designed by SOM, 100 Mount Street, a 34-story office tower located in North Sydney, carries an expressive braced frame as its lateral system [12]. What sets it apart from other braced frames is that the frame of 100 Mount Street is braced at three-quarter points instead of midpoints, displayed in Fig.2-2. When determining the optimal location of bracing, topology optimization, under the objective of maximizing structural stiffness, will choose its bracings at the three-quarter points [13]. However, this bracing configuration will cause discontinuity for structural members, potentially incurring higher cost and more difficulty in installation. SOM still proceeds with the optimized design because it out-performs traditional braced frame.

11
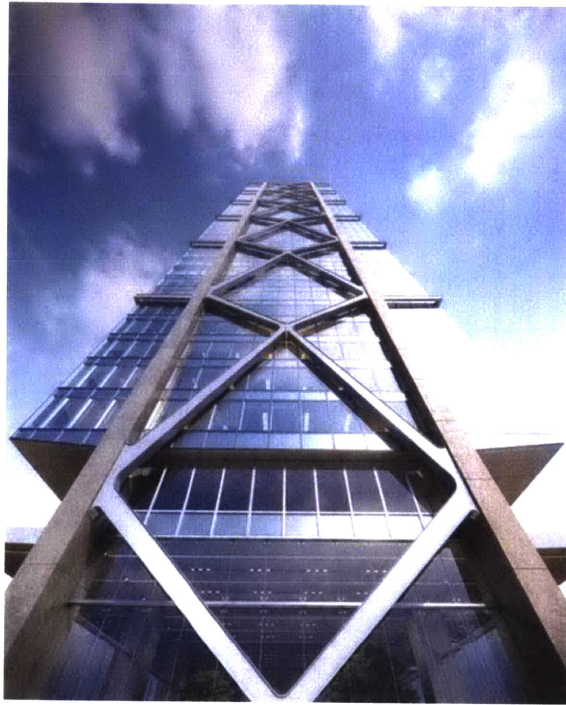
Fig.2-2 Braced frame of 100 Mount Street in Sydney

Contrasting to the fast development of topology optimization algorithms and computational models, applications of topology optimization in civil structures is also severely limited by the lack of experimental endorsement of algorithms. Only a few attempts have been made to fabricate the designs and validate the results. Four researches highlighted below have taken the initiative and produced prototypes for experiments.

Lopez, Van Mele and Block, in their paper *"Design, fabrication and testing of a prototype, thin-vaulted, unreinforced concrete floor"*, detailed the necessary procedures of an application of optimization [7]. They started with form-finding of a bounded floor slab which translated to the optimized geometry displayed in Fig.2-3. They then described the fabrication and testing process; an example of the testing setup is displayed in Fig.2-4. The authors proceeded further by comparing the experimental deflections to the allowable deflection established by structural codes. They successfully demonstrated that this optimized floor slab performed adequately in serviceability and ultimate strength while reducing material usage.

On the contrary, the form-finding technique the authors used is not topology optimization. In addition, their compressive and bending test results varies, which speaks to the mercurial nature of concrete as a composite material. Nevertheless, their experiment

provides a solid foundation for future researches and gives rise to the endless possibilities that optimized structural components have the potential to meet and even surpass requirements.
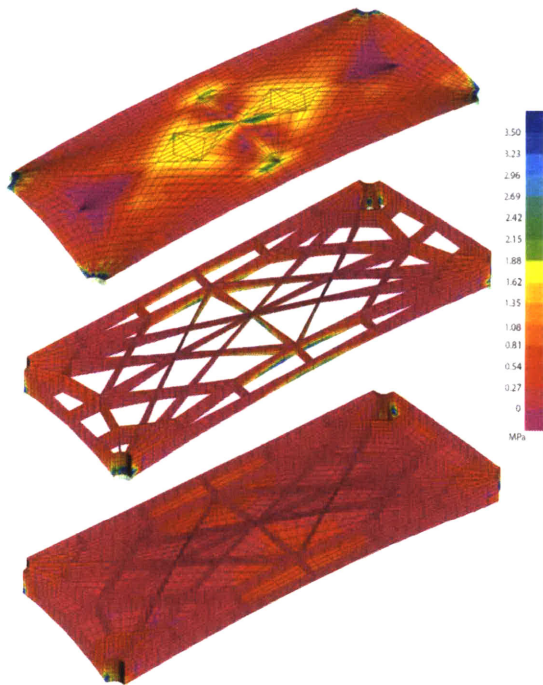
Fig.2-3 FE model of the optimized floor slab   Fig.2-4 Testing of the optimized floor slab
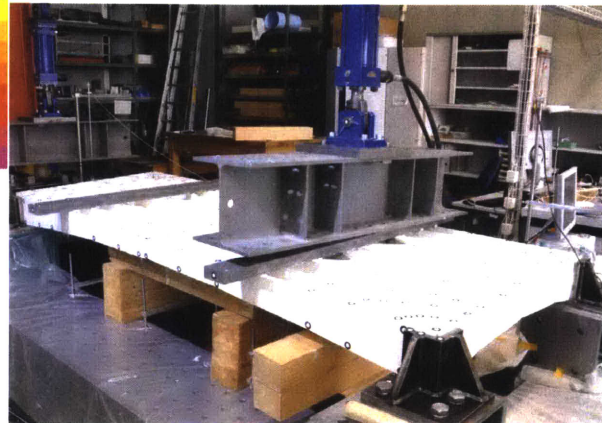
Dombernowsky and Søndergaard, in their paper "*Design, analysis and realisation of topology optimized concrete structures*", presented a fabricated prototype of a topology optimized shell structure using large CNC milling machine [6]. The authors extensively explored the practicality of topology optimization as a design tool to facilitate the form-finding process, and the result is an architecturally expressive reinforced concrete structure, displayed in Fig.2-5. Their work shows the versatility of topology optimization and its free-form nature.

On the contrary, the authors used traditional methods for designing the reinforcement within the optimized concrete phase. This shows the disconnection between optimization and traditional methods of analysis, between concrete and its reinforcement. Lastly, no test was performed to validate that the actual displacement matches the prediction of their analytical model.

Fig.2-5 Finalized prototype concrete shell structure

The third research, by Jackson Jewett and Josephine Carstensen, titled "*Topology-optimized design, construction and experimental evaluation of concrete beams*", used topology optimization as its primary form-finding tool [8]. The authors chose the 4-point bending configuration as their design domain, constructed and compared the performance of plain concrete beams under two different objectives, minimize compliance and volume. The results of the minimum compliance model are displayed in Fig.2-6. Their testing setup is displayed in Fig.2-7. Their results show that the beams optimized for compliance failed at higher loads while exhibiting brittle behavior. Unlike the second research where scholars employed a two-step process, optimizing the concrete phase while using traditional reinforcement, the authors of this paper completely discarded the reinforcement phase and directly targeted the validity of the continuum optimization algorithm.
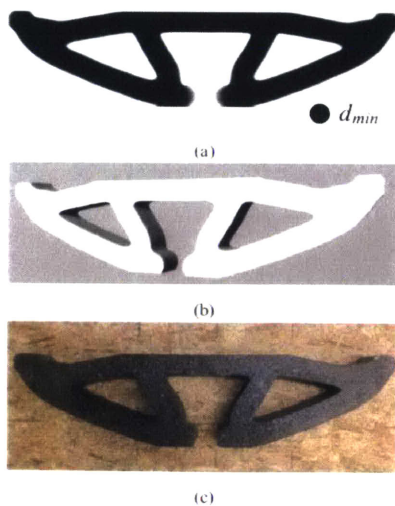
Fig.2-6 Topology Optimized Design

Fig.2-7 Testing of the Optimized Beam

14

Before discussing the last research, it is worth highlighting the research done by Dr. Gaynor, titled "*Reinforced Concrete Force Visualization and Design Using Bilinear Truss-Continuum Topology Optimization*", which forms the theoretical basis of this research [5]. Dr. Gaynor's research focused on the implementation of Strut-and-Tie Model (STM) for reinforced concrete beam design which the hybridity originates from a truss element ground structure incorporated within the density-based continuum topology optimization framework. The resultant optimized truss elements represent the tensile load path whereas the optimized continuum structure indicates the compressive load path. The details will be discussed more in later sections. There are also numerous other researches specifically targeting on the development of topology optimization using STM, and a full review of their methods is beyond the scope of this paper [14][15][16].

The last research, by Jackson Jewett and Josephine Carstensen, titled "*Experimental investigation of strut-and-tie layouts in deep RC beams designed with hybrid bilinear topology optimization*", is the most pertinent to this research [9]. The authors also adopted Gaynor's Hybrid Truss-continuum algorithm [5], and they investigated the complexity of the optimized reinforcement and how it could affect the strength of the beams. Two different complexities of reinforcement were designed, manufactured, and tested, displayed in Fig.8. The results of the experiments show that increasing the complexity of the reinforcement from Fig.2-8 (a) to (b) does not greatly increase the strength of the beams. This paper positively influences the choice of reinforcement complexity of this research which will be detailed in later sections.

(a)   (b)
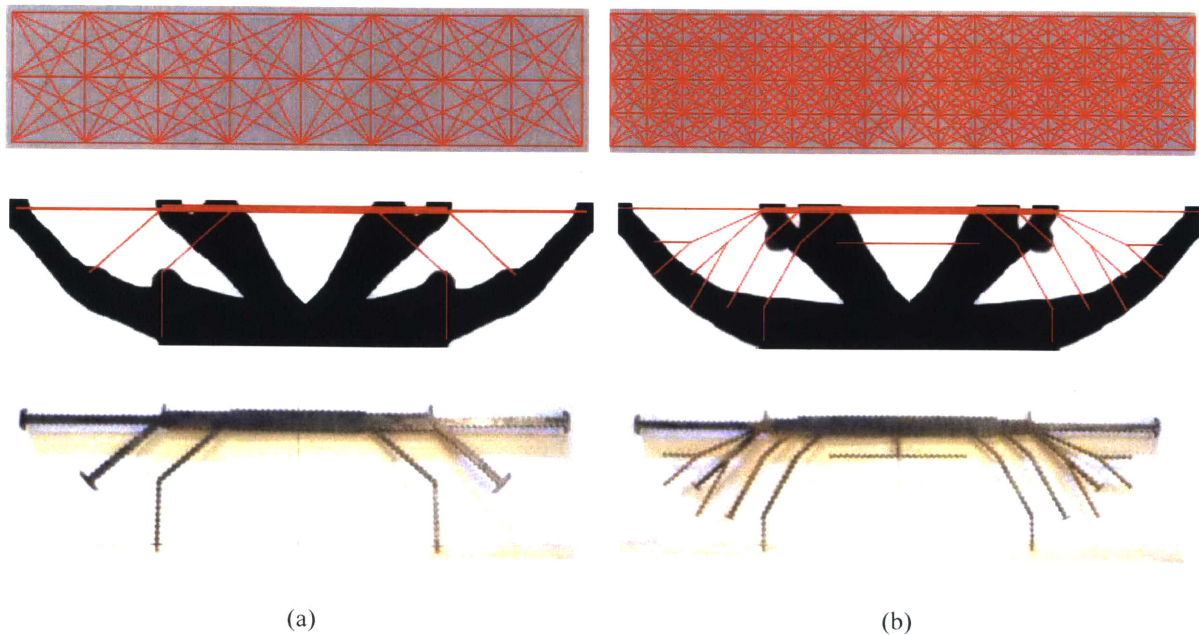
Fig.2-8 Different complexities of optimized reinforcement, designed and manufactured

15

3. Methodology

3.1 General setup

Gaynor's optimization algorithm provides the basis for this paper [5]. He adopts a density-based approach and uses Method of Moving Asymptotes (MMA) as the gradient-based optimizer [17]. The algorithm also operates with a hybrid mesh that contains both truss and continuum elements where the truss elements are designed to take tension and the continuum elements are designed to take compression. The continuum ground structure is finely meshed into individual continuum elements, each of which is associated with a density ρ^e. ρ^e can take any value between 0 and 1, 0 being a void element and 1 being a solid element. The truss ground structure is built based on the nodes of the continuum element, and this process will be discussed in greater details later. Interested readers are referred to Gaynor's paper [5] for more details.

The design domain chosen for this research is a simply-supported beam with a single point load in the middle, displayed in Fig.3-1. The size of the design domain is chosen to be: L = 3 feet, H = 9 inches to work best with the size of the loading machine. The width of the beam is chosen to be 2 inches. The deep beam criterion is specified in ACI 318 chapter 9.9 and the size of the design domain is chosen to comply with this criterion [18]. Hence a strut-and-tie model is appropriate for analyzing and designing this configuration. A 20-kip point load is chosen.
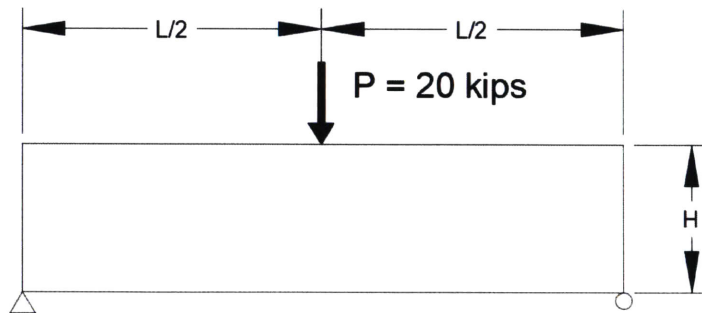
Fig.3-1 Design domain with loading and support conditions

3.2 Stress Dependent Hybrid Mesh

The hybridity results from a combined mesh of continuum and truss elements. Fig.3-2-1 displays an example hybrid mesh by Gaynor with 12x12 continuum elements and completely connectivity of the truss elements [5]. In this case, the truss elements are connected at every 4

continuum elements. Transfer of forces only happens at the nodes where the continuum and truss element coincide. Researchers have the freedom to control the complexity of the truss mesh by specifying the number of continuum elements that the truss elements skip as well as their connectivity. A coarser mesh work better for manufacturability purpose while a finer mesh might provide a better objective value.
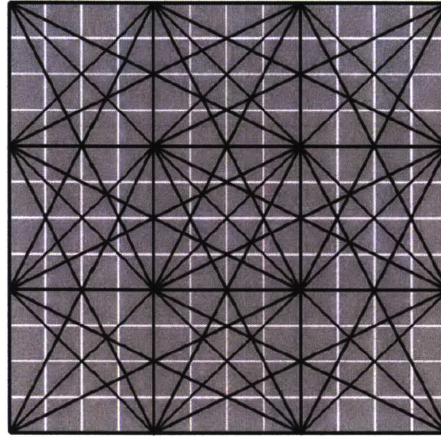
Fig.3-2-1 Hybrid mesh of truss and continuum elements

The bilinear stress-strain properties of steel and concrete is assumed and Fig.3-2-2 below displays the relationships. The Modulus of Elasticity of concrete is assumed to be 3,600 ksi in compression and 290 ksi in tension. The Modulus of Elasticity of steel is assumed to be 29,000 ksi in tension and 0 in compression to ensure that when the force is transferred, the truss elements only carry axial tension. It is important to grant concrete tensile strength to maintain positive-definiteness of the global stiffness matrix [5].
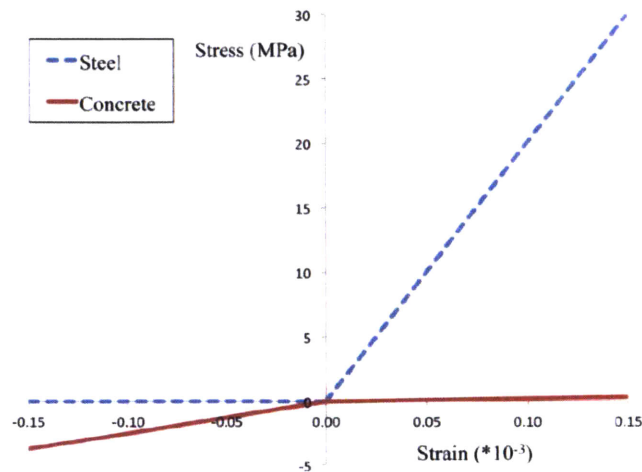
Fig.3-2-2 Material bi-linearity of steel and concrete

17

3.3 Minimum compliance

The general problem formulation for a minimum compliance objective can be expressed as:

$$min \qquad f(\rho) = F^T d$$
$$subject\ to: \quad K(\rho)d = F$$
$$\sum_{e \in \Omega} \rho^e v^e \leq V$$
$$\rho^e_{min} \leq \rho^e \leq \rho^e_{max} \ \forall\ e \in \Omega \qquad (1)$$

An optimization problem formulation needs to include an objective function and a set of constraints. In this project, the objective is to minimize compliance, which is the same as maximizing stiffness within the elastic range. The objective value f is calculated as the product of the external load vector F and the resultant displacement d vector from equilibrium. The constraints are: 1) the structure must be in equilibrium under the given loads, and 2) volumetric constraint. The matrix K denotes the global stiffness matrix of the design domain, ρ^e denotes elemental material density, V denotes the upper limit of allowable volume, and Ω denotes the design domain. A small positive number is selected for ρ_{min} to maintain the positive definiteness of the stiffness matrix.

3.4 Changes in constraints

This is the original problem formulation used by Gaynor [5]:

$$min\ f(\rho) = F^T d$$
$$subject\ to: K(\rho)d = F$$
$$\sum_{e \in \Omega_t} \rho^e_t v^e_t + \sum_{e \in \Omega_c} \rho^e_c v^e_c \leq V$$
$$0 \leq \rho^e_t \ \forall\ e \in \Omega_t$$
$$0 \leq \rho^e_c \leq 1 \ \forall\ e \in \Omega_v \qquad (2)$$

Gaynor's volume constraint consists of two components, the volume of the truss (i.e. steel reinforcement) and the volume of concrete. The two volumes are bounded by a single upper bound V. In order to enable control of the volumetric amount of concrete in the design domain, this general volume constraint that includes both the steel and the concrete portion is separated into 2 individual constraints, one representing steel and one representing concrete. The new problem formulation, thus, becomes the following:

18

$$min\ f(\rho) = F^T d$$

$$subject\ to: K(\rho)d = F$$

$$\sum_{e\in\Omega_t} \rho_t^e v_t^e \leq V_t$$

$$\sum_{e\in\Omega_c} \rho_c^e v_c^e \leq V_c$$

$$0 \leq \rho_t^e \ \forall\ e \in \Omega_t$$

$$0 \leq \rho_c^e \leq 1 \ \forall\ e \in \Omega_v \tag{3}$$

Since the constraints have changed, different sensitivities should be derived for each of them. The derivation of sensitivities will be detailed in later sections. In this research, the following volume fractions are explored: 75%, 85%, 90%, 95%, and 100%. For the volume fractions between 75% and 95%, two beams per fraction will be fabricated and tested. For the 100% full volume, four beams will be fabricated and tested, two of which will have traditional reinforcement and the other two will carry the optimized reinforcement from the results of the 75% volume fraction.

3.5 Traditional strut-and-tie model

The controlled volume of steel is obtained using the traditional analysis of a Strut-and-Tie Model. In Fig.3-5 we can see the desired simply-supported beam with a 20-kip point load at midspan. According to chapter 9.9 of ACI 318, the entire design domain can be characterized as D-region [18]. D region denotes the region where reinforcement can be designed using Strut-and-Tie Model. The thickness of the beam is chosen to be 2 inches. Assuming the effective depth of the beam is 0.9h, then the maximum design shear capacity allowed per ACI 318:

$$\phi Vn = \phi 10\sqrt{f_c'}b_w d = 92.2\ kips \tag{4}$$

$f'c$ notes the compressive strength of the concrete, b_w is the width of the beam and d is the depth of the beam. The shear capacity is greater than the shear demand $V_u = 10\ kips$. Thus, we can proceed forward with the design. The strut-and-tie model, with the simplest determinate truss within the design domain and the associated axial forces, is displayed below as Fig.3-5.
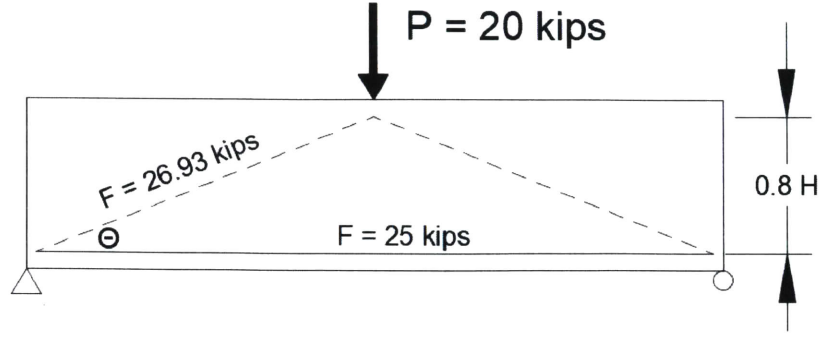
Fig.3-5 Strut-and-tie model

Dashed line – compression strut, solid line – tension tie

The bottom angle θ can be calculated as:

$$\theta = tan^{-1}(\frac{0.8\,H}{0.5\,L}) = 21.8\ degrees$$

It is usually advisable for theta to be greater than 25 degrees [4], but it will not affect our design since we are using this model only to obtain the cross-sectional area of the tie which will lead to the controlled volume of the reinforcement. We can calculate the forces within each member of the truss and we obtain the force in the bottom chord to be 25 kips. With a safety factor = 0.75, and the yield strength of the steel assumed as 54 ksi [19], we can obtain the cross-sectional area of the tie:

$$A_{ts} = \frac{F}{\phi F_y} = \frac{25\ kips}{0.75 * 54\ ksi} = 0.62\ in^2$$

Thus, the controlled volume of steel can be calculated as:

$$V_s = A_{ts} * L_x = 0.62\ in^2 * 36\ in = 22.32\ in^3 \tag{5}$$

This number will be used as the upper limit of the steel in the optimization algorithm.

3.6 SIMP

Solid Isotropic Microstructure with Penalization (SIMP) was first introduced by Bendsoe and Sigmund in 1999 [20] and a brief overview is provided below. Its main function is to convert the optimization from a discrete to a continuous problem. This is desirable since continuous optimization problems can be solved using gradient-based optimizer. The relationship can be described mathematically as:

$$K^e = ((\rho^e)^\eta + \rho^e_{min})K^e_0 \tag{6}$$

20

K^e is the penalized stiffness of the element e. By raising the elemental density ρ^e to a certain power η, its stiffness is dramatically reduced from the original linear interpolation ($\eta = 1$). It is also desirable to have the element densities converge to either 0 or 1, thus, higher powers of η are used. This is a necessary step to tell the optimizer that it is no longer optimal to put intermediate density material because its stiffness is not linearly proportional to its density. The coefficient $\eta = 4$ is chosen for this research. Interested readers are referred to Bendsoe and Sigmund's paper [20] for more details on the implementation of SIMP.

3.7 Filtering of element densities

A filtering method is implemented to prevent numerical instabilities. The underlying principle is that an element's density is no longer determined independently but is a weighted average within its neighborhood. Fig.3-7-1 below displays this principle that the density of the element highlighted in the center of the circle Ω_w^e is dependent upon all the elements within the neighborhood Ω_w^e [21].
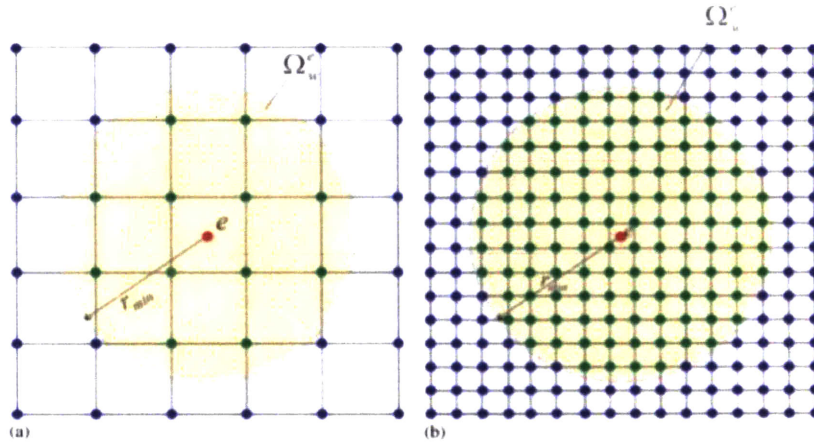
Fig.3-7-1 Filtering (Guest et al. 2004)[21]

The weighting function can be a standard linear relation, mathematically formulated as:

$$w(x_i - x_e) = \begin{cases} \dfrac{r_{min} - \left\| x_i - x_e \right\|}{r_{min}} & if\ i \in N^e \\ 0 & if\ otherwise \end{cases} \qquad (7)$$

r_{min} is the radius of the neighbor specified by the researcher, x_e is the location of the centroid of the element of interest, and x_i is the location of centroid of the neighboring elements. Thus, from the above formulation we can see that if the neighboring element falls outside of the

21

neighborhood, i.e the distance between the centroids of the two elements is larger than the specified r_{min}, it does not have an effect on the density of the element of interest.

This research utilizes a filtering technique called Heaviside Projection Method with $\beta = 20$ for numerical stability. The Heaviside Projection Method is first proposed by J. Guest in 2004 [21]. Reader is referred to this paper to detailed explanation.

The radius of the circle, often referred to as the minimum length scale, can be specified by the user. In this research, the minimum length scale is set to be 1 inch. The impact of the minimum length scale is displayed below:

Fig.3-7-2 75% volume fraction with a minimum length scale of 1 inch

Fig.3-7-3 75% volume fraction with a minimum length scale of 2 inches

Fig.3-7-2 depicts the result of an optimized beam with 75% volume fraction with a minimum length scale of 1 inch, and Fig.3-7-3 depicts that of a beam with minimum length scale of 2 inches. As we can observe, the choice of minimum length scale of the user can make
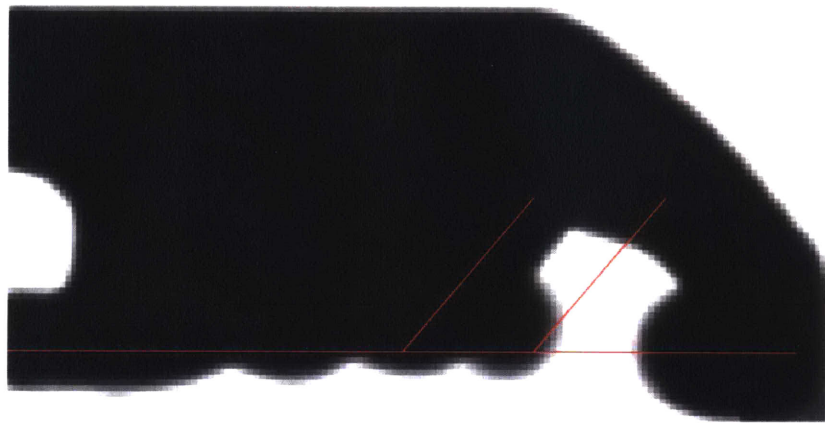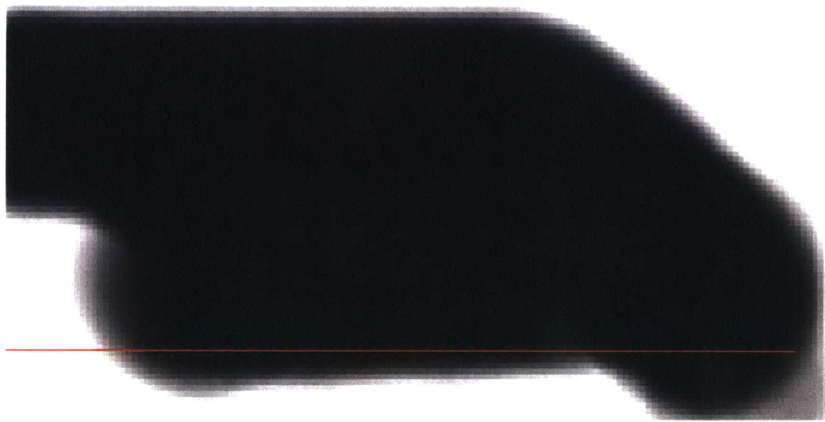
a significant impact on the optimization results. The choice of 1 inch is based on the resulting geometry and manufacturability constraint.

3.8 Sensitivities

In order for a gradient-based optimizer, such as MMA [17], to function efficiently, the derivatives of the objective function f and the associated constraints c should be calculated and provided to the optimizer. They are mathematically formulated as:

$$\frac{\partial f}{\partial \phi_i} = \sum_{e \in \Omega} \frac{\partial f}{\partial \rho^e} \frac{\partial \rho^e}{\partial \phi_i}$$

$$\frac{\partial c}{\partial \phi_i} = \sum_{e \in \Omega} \frac{\partial c}{\partial \rho^e} \frac{\partial \rho^e}{\partial \phi_i} \tag{7}$$

ρ^e denotes element densities and ϕ_i is the unfiltered densities or the design variables. The sensitivities are calculated using the Adjoint Method [22]. As defined in section 3.7, the partial derivatives of ρ^e with respect to ϕ^e can be calculated as:

$$\frac{\partial \rho^e}{\partial \phi_i} = \frac{w(x_i - x_e)}{\sum_{i \in N^e} w(x_i - x_e)} \; [21] \tag{8}$$

Furthermore, the sensitivity of the compliance objective function f with respect to element densities ρ^e can be calculated, after penalization of intermediate stiffness using the SIMP method discussed above, as:

$$\frac{\partial f}{\partial \rho^e} = -\eta(\rho^e)^{\eta-1}(d^e)^T K_0^e d^e \tag{9}$$

The sensitivities of the two constraints, the volumetric constraints of steel and concrete, can be calculated as:

$$\frac{\partial c_1}{\partial \rho^e} = L_t^e$$

$$L_t^e - length\ of\ the\ truss\ elements$$

$$\frac{\partial c_2}{\partial \rho^e} = V_c^e \tag{10}$$

$$V_c^e - volume\ of\ the\ continuum\ elements$$

23

3.9 Truss ground structure

There are a number of ways that we can describe the configuration and the connectivity of the truss ground structure that is housed within the continuum ground structure. The truss nodes are a selective group of the continuum nodes. The bottom chord of the truss ground structure is set to start from the bottom boundary of the continuum mesh at a distance:

$$d = \text{L}_{cover} + d_{tie}$$

L_{cover} is the cover distance and it is chosen as $\text{L}_{cover} = 0.8$ in. d_{tie} is half of the depth of the tie obtained from the traditional strut-and-tie model and it is calculated as d $= 0.62$ in. In both directions, the truss connectivity is setup such that one bay is defined by skipping a number of continuum nodes. To reiterate, the size of the design domain, utilizing structural symmetry, is $18''$ by $9''$, and the size of the mesh is 200 x 100. The ratio between the two has to match. In the longitudinal direction, every bay of truss skips 37 nodes, and the in the transverse direction, every bay of truss skips 33 nodes. The number of skipped nodes is obtained from the research done by Jewett and Carstensen [9]. Fig.3-9-1 and Fig.3-9-2 below demonstrate the different connectivity patterns that we have the freedom to control. This research chose the complete connectivity pattern as displayed in Fig.3-9-2.
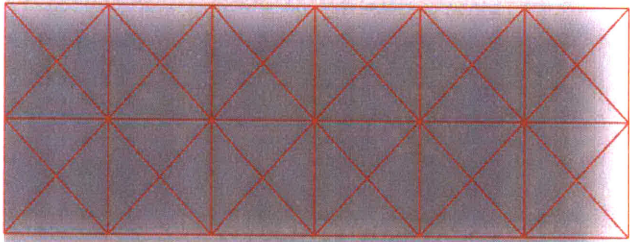
Fig.3-9-1 Local Connectivity for Truss Ground Structure
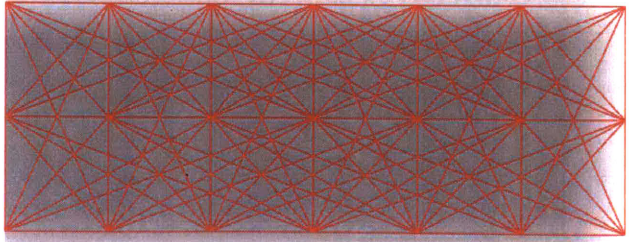
Fig.3-9-2 Complete Connectivity for Truss Ground Structure

24

3.10 Enforcing a minimum diameter

In order for the filter to work unbiased for every continuum element, the weights of the elements around the boundaries need to be adjusted since they cover less elements within 1 filter radius (the set minimum length scale). For simplicity purposes, the ϕ of the elements around the boundary within 1 filter radius is eliminated. In addition, a strip of elements that is defined by the interior edge of the removal region of the right boundary overlapping with the removal region of the bottom boundary is added back to ensure the solidity of the elements near the support. Fig.3-10-1 and Fig.3-10-2 below demonstrate the effect of prescribed phi on the weight distribution of the continuum elements. This research proceeded with the pattern displayed in Fig.3-10-2.
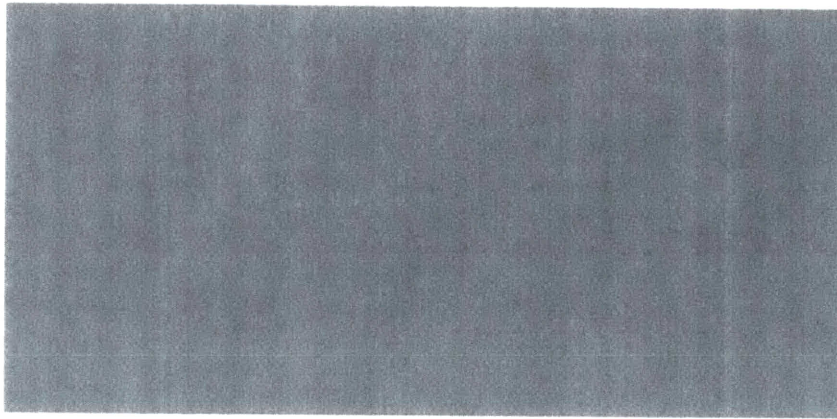
Fig.3-10-1 Uniform ϕ across the entire domain
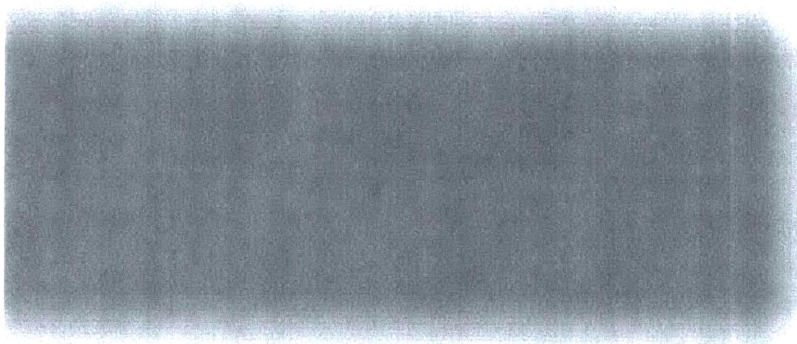
Fig.3-10-2 ϕ removed around the boundaries with the addition of the strip

3.11 Computational model results

The results of the optimization, utilizing structural symmetry for volume fraction 75%, 85%, 90%, and 95%, are displayed in Fig.3-11 below. Although the optimized reinforcement appears as line elements in the figure, a separate file is created that saves the connectivity and cross-sectional area information. These files need to be post processed to obtain the correct geometry of the reinforcement.

(a)

(b)

(c)

(d)
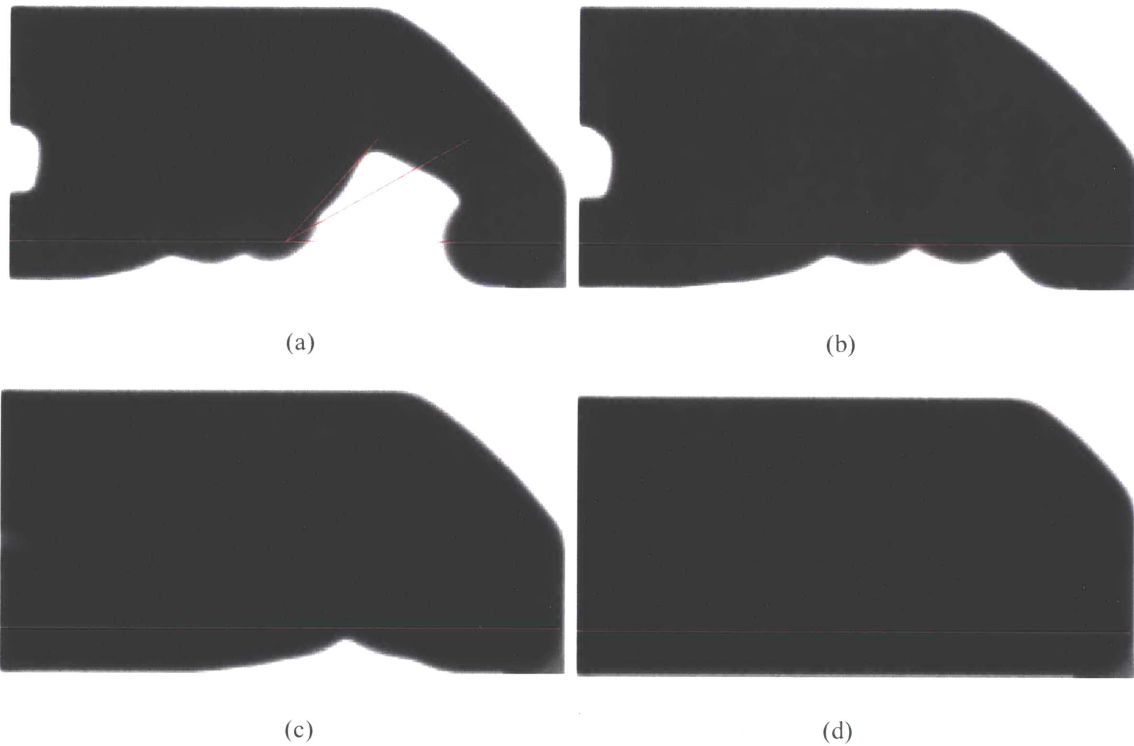
Fig.3-11 (a) optimized result for 75% volume, (b) optimized result for 85% volume, (c) optimized result for 90% volume, (d) optimized result for 95% volume

As we can observe, the optimized result of 75% volume fraction has a distinctive reinforcement layout than that of the others. All of the designs have strictly the same volume of reinforcement.

3.12 Prepare digital files for steel manufacturing

The optimized tie output is saved in a separate .txt file containing crucial information that describes the connectivity and the cross-sectional area of the tie. The information is post processed using Grasshopper to convert into rhino geometry. Fig3-12-1 below displays the Grasshopper script.
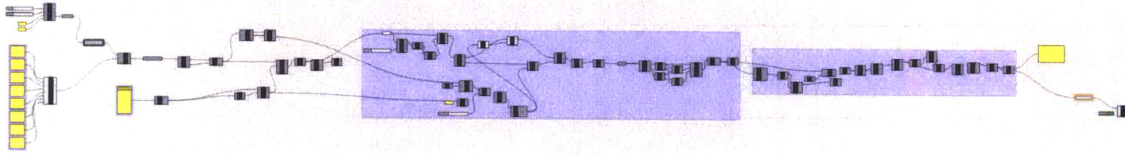
Fig.3-12-1 Grasshopper script

Corrugations are added to the edges of the reinforcements to enhance the bonding to the concrete. The corrugations do not increase the depth of the reinforcement. Anchors are also added to the ends of the reinforcement and the area of the anchors is chosen to comply with the requirements of ACI [18]. Fig.3-12-2 below displays the optimized post-processed reinforcement configuration for the beams. Lastly, the rhino geometries are prepared for the waterjet machine.
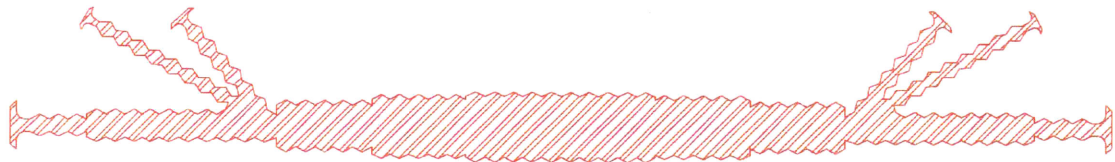
(a) optimized reinforcement of 75% volume

(b) optimized reinforcement of 85% volume

(c) optimized reinforcement of 90% volume

(d) optimized reinforcement of 95% volume

(e) traditional reinforcement of 100% volume

Fig3-12-2 Configuration of steel reinforcement for different concrete volume

27

3.13 Manufacturing of the reinforcement

Manufacturing of the reinforcement is done in MIT's architecture lab where the reinforcement patterns are cut out of steel plates using waterjet. The steel plates are 3 feet by 6 inches by 0.5 inches and they have a yield strength of 54 ksi [19]. In order for the waterjet machine to not cut open the plate and release its internal stresses, the optimized reinforcements are shortened to 34.5 inches long. It is advisable to manufacture the reinforcement out of slight longer steel plates for future researches. Fig.3-13 below displays the final products:
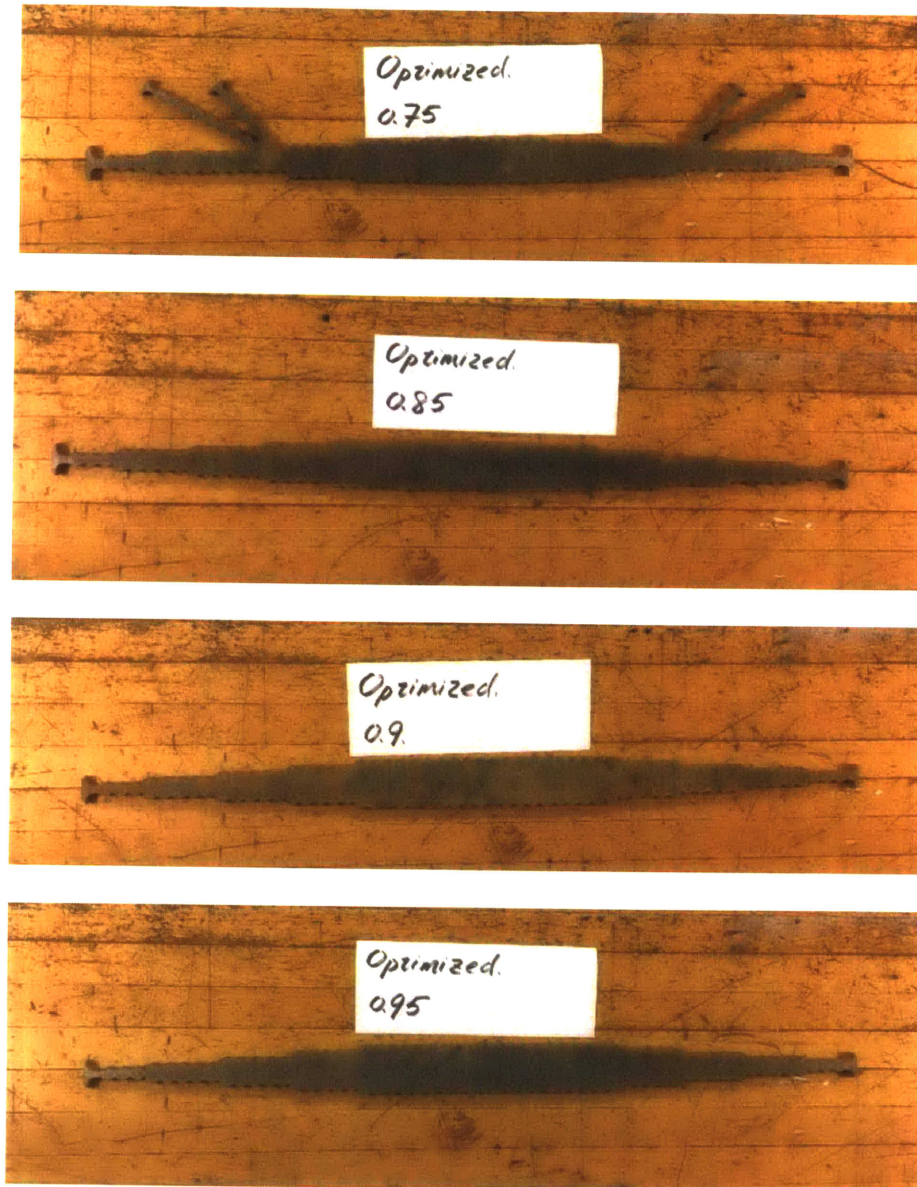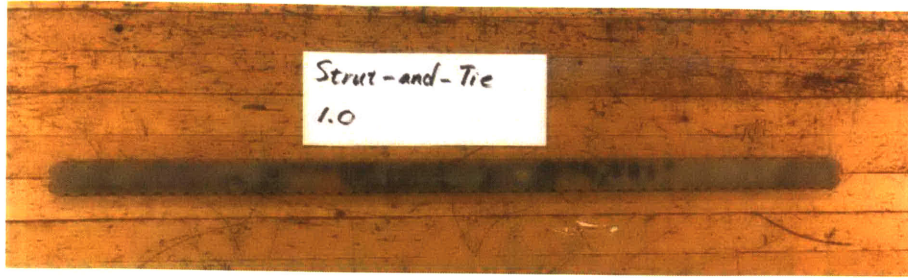
Fig.3-13 Manufactured reinforcement for different volumes

3.14 Manufacturing of the concrete molds

Manufacturing of the concrete molds is done using CNC milling into styrofoam. The optimized continuum domain is saved to vtk. files exported by matlab. Then the vtk. files are converted to stl. files via a matlab script. The stl. files are process through Rhino [23] to make cutting files for the CNC machine. Fig.3-14 below displays the rhino models as well as the final products:
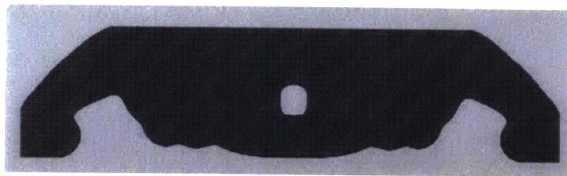
(a) Optimized continuum 75% volume
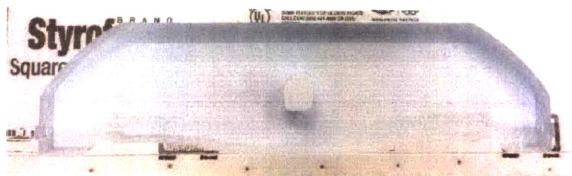
(b) Optimized continuum 85% volume
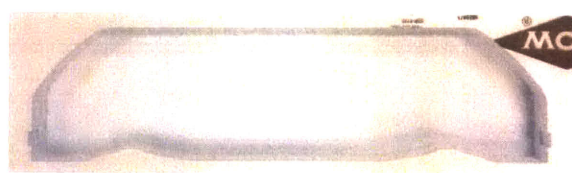
(c) Optimized continuum 90% volume
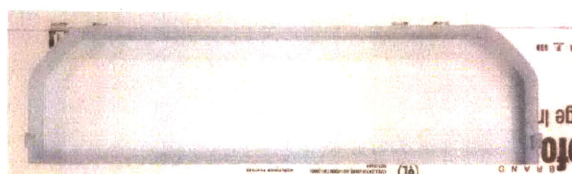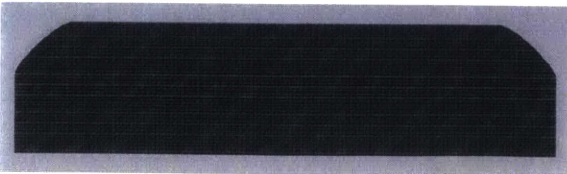
(d) Optimized continuum 95% volume

Fig.3-14 Rhino models and the manufactured molds

29

3.15 Concrete mix design

Obtaining the correct Modulus of Elasticity of concrete is crucial to safeguard the validity of the experimental results. The Modulus of Elasticity of concrete is chosen to be 3,600 ksi and it can be calculated from the compressive strength of concrete, per ACI 318-14 19.2.2 [18], as:

$$E_c = w_c^{1.5} 33\sqrt{f_c'}$$

For normal weight concrete, the formula can be simplified as:

$$E_c = 57,000\sqrt{f_c'}$$

Thus, we can back calculate the compressive strength of our concrete to be 4 ksi. To design a 4 ksi concrete mix, this research uses the book "*Civil Engineering Materials*" by Peter A. Claisse [24]. Due to the limited space of the design domain, only concrete mortar, a mix that only contains water, cement, and fine aggregates, is designed and used. The ratios are displayed in table 3-15 below:

Water-to-cement ratio	0.575
Sand-to-cement ratio	3.28

Table 3-15 Concrete mix design, ratios among different materials

3.16 Preparation for casting.

To limit imperfections caused by reinforcement placement, the steel layouts are hanged using wires and wooden dowels from the surface of the mold to position the piece correctly. The depth of the beam is 2 inches, and the depth of the manufactured reinforcement is 0.5 inches, thus a 0.75-inch gap is left from the bottom, demonstrated in Fig.3-16-1. To ensure stability and eliminate accidental twist, the reinforcement is hanged 4 times throughout its length. Fig.3-16-2 below displays the assembly ready to be casted.
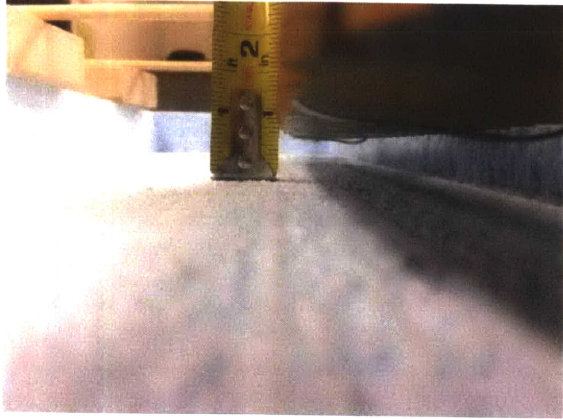
Fig.3-16-1 Depth quality control   Fig.3-16-2 Assembly
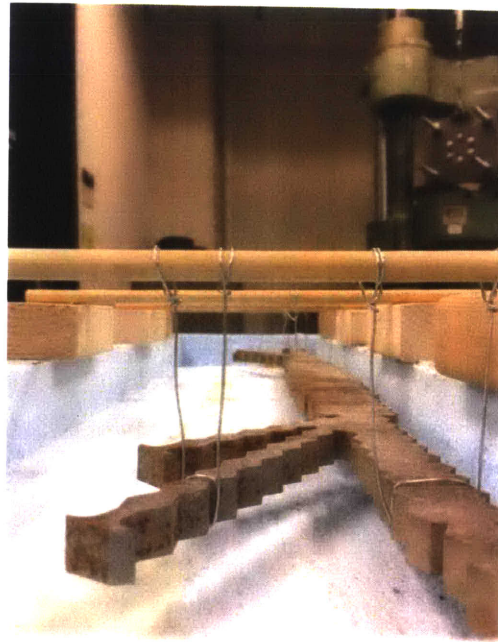
A total of 4 batches are required to cast all the 12 beams. To ensure a confident level of uniformity of concrete strength across different batches and minimize errors due to port batches, each batch will contain beams with different volumes and designs. The batch information is detailed in table 3-16-1 below:

Batches	Volume ratios		
1st	85%	95%	100% (regular reinforcement)
2nd	90%	95%	100% (optimized reinforcement)
3rd	75%	85%	100% (regular reinforcement)
4th	75%	90%	100% (optimized reinforcement)

Table 3-16-1 Batch information

Slump results are displayed in table 3-16-2 below:

	Batches			
	1st	2nd	3rd	4th
Slump (cm)	2.2	2	3	3.5

Table 3-16-2 Slump for each batch

The slump that this research is targeting $3 - 4$ inches for the desired compressive strength, according to Claisse [26]. The beams are demolded after 2 days and placed in a pool to hydrate for 26 days.

3.17 Beams ready to be tested

Fig.3-17 below displays the finished products, the beams that are ready to be tested.

(a) beam with full volume

(b) beam with 95% volume

(c) beam with 90% volume
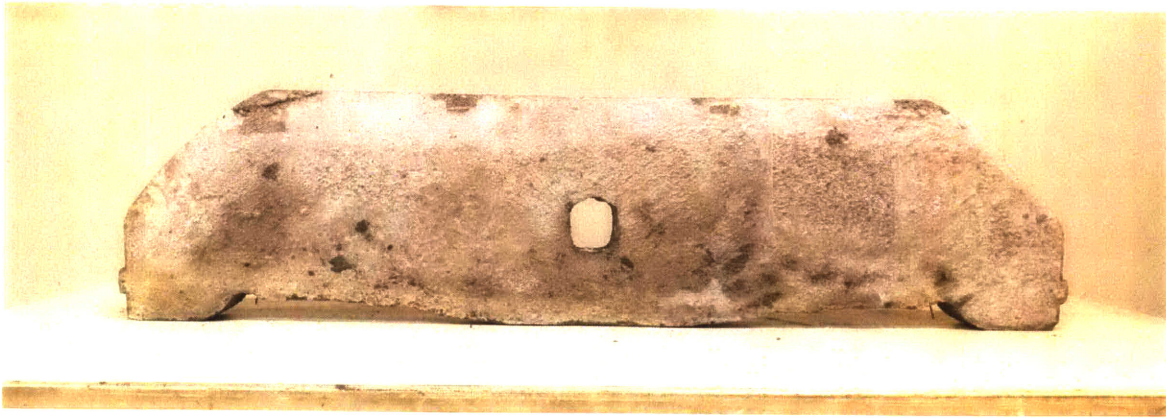
(d) beam with 85% volume
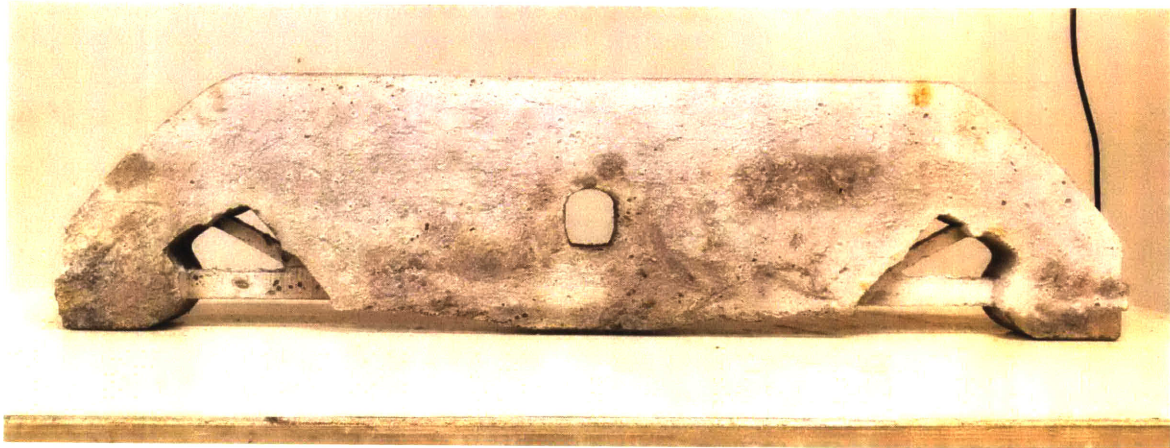
(e) beam with 75% volume

Fig.3-17 Finished beams that are ready to be tested

4. Experimental set-up

Fig.4 Experimental set-up for beam testing

All the beams were experimentally tested on a Baldwin Universal Testing Machine (UTM) using deflection control. The beams were simply supported at the ends using a simulated pin and roller, and loaded with a point load at mid-span. The point load was transmitted through a small piece of intermediate steel bar to the beams from the circular plate of the machine. Fig.4 displays the experimental set-up for a beam with 75% volume. A small pre-load is introduced to ensure stability of the beams, which will be corrected during post-processing. The beams were loaded until failure was detected by the machine. The machine measures load and position at each incremental deflection.

The concrete cylinders were tested on the Baldwin Universal Testing Machine (UTM) using load control. Two extensometers were mounted onto the cylinders to accurately capture their displacements and obtain their Modulus of Elasticity. Results were recorded from the two extensometers at each incremental load. Only the compression tests were performed.

5. Experimental results

5.1 Concrete cylinder results

Batch 1	f'c (kPa)	f'c (ksi)	Batch 2	f'c (kpa)	f'c (ksi)
Sample 1	29390	4.26	Sample 1	24238	3.52
Sample 2	26052	3.78	Sample 2	27124	3.93
Sample 3	27142	3.94	Sample 3	24383	3.54
Average		3.99	Average		3.66

Batch 3	f'c (kpa)	f'c (ksi)	Batch 4	f'c (kpa)	f'c (ksi)
Sample 1	29736	4.31	Sample 1	25262	3.66
Sample 2	27282	3.96	Sample 2	26991	3.91
Sample 3	28230	4.09	Sample 3	29101	4.22
Average		4.12	Average		3.93

Table 5-1 Concrete cylinder results – compressive strength

Table 5-1 displays the compressive strength of each batch with the results highlighted in red and. The assumed compressive strength (f'_c) of concrete was 4 ksi, and using the equation from ACI [18], the desired Modulus of Elasticity for normal-weight concrete can be obtained:

$$E = 57,000\sqrt{f'c} = 3,600 \ ksi$$

As can be observed in Table 5-1, the compressive strengths of the cylinders are adequately within the acceptable neighborhood of 4 ksi with -1.8 – 3% variation. The compressive strength of the second batch is an outlier with 8.5%.

Modulus of Elasticity (*ksi*)			
Batch 1	Extens 1	Extens 2	Average
Sample 1	2806.03	3593.01	3199.52
Sample 2	4960.18	2197.64	3578.91
Sample 3	2574.62	3752.33	3163.47
Average			3313.97

Modulus of Elasticity (*ksi*)			
Batch 2	Extens 1	Extens 2	Average
Sample 1	3845.94	2017.99	2931.97
Sample 2	3290.68	2155.81	2723.24
Sample 3	1741.76	3059.59	2400.67
Average			2685.29

Modulus of Elasticity (*ksi*)			
Batch 3	Extens 1	Extens 2	Average
Sample 1	2629.28	2873.89	2751.59
Sample 2	3062.80	2431.21	2747.01
Sample 3	2534.23	2797.09	2665.66
Average			2721.42

Modulus of Elasticity (*ksi*)			
Batch 4	Extens 1	Extens 2	Average
Sample 1	2173.89	3149.22	2661.55
Sample 2	2346.92	2746.87	2546.89
Sample 3	2916.15	2913.89	2915.02
Average			2707.82

Table 5-2 Concrete cylinder results – Modulus of Elasticity

Table 5-2 displays their Modulus of Elasticity highlighted in red as well. However, the Modulus of Elasticity varies and is generally noticeably lower than the value assumed within the design. For most batches, a 25% decrease of stiffness is observed. The results are summarized succinctly in Table 5-3.

	E (*ksi*)	Error
Target	3600.00	
Batch 1	3313.97	7.9%
Batch 2	2685.29	25.4%
Batch 3	2721.42	24.4%
Batch 4	2707.82	24.8%

Table 5-3 Summary of Modulus of Elasticity

The satisfactory compressive strength of the concrete batches is most likely obtained by keeping the water-to-cement ratio rigorously according to recommendation [24]. It is believed that the variation within the experimentally observed Moduli of Elasticity occurs because all the coarse aggregates are replaced with fine aggregates for workability purpose of the design domain.

5.2 Beam Results
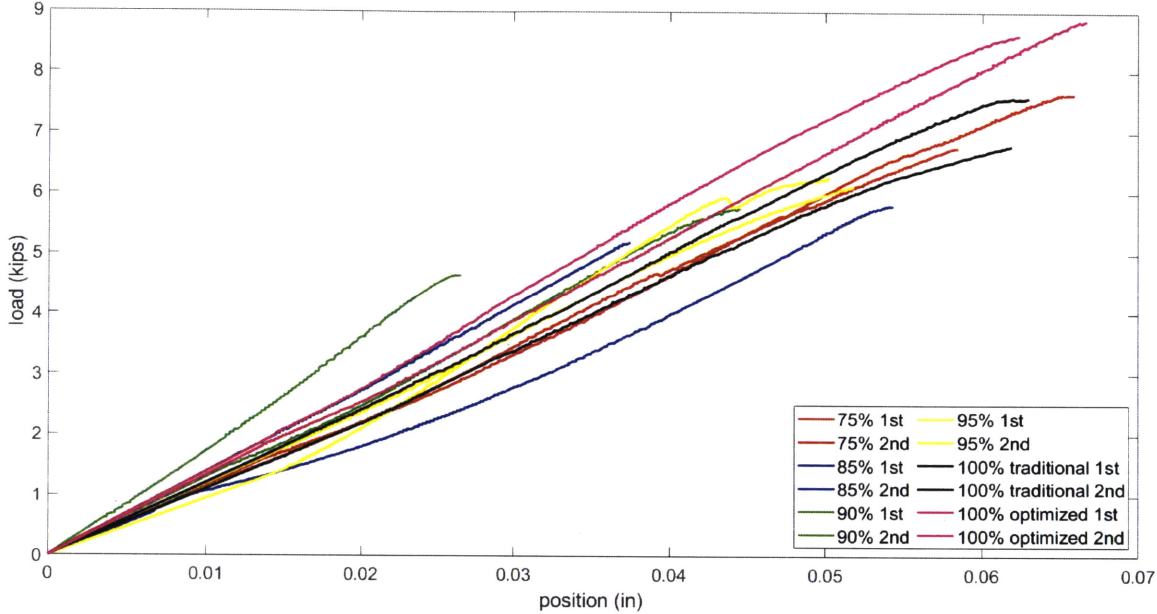
Fig.5-2-1 Experimental results of concrete beams with varying volume fractions

The experimentally obtained load vs. displacement curves for all tested beams are plotted in Fig.5-2-1. The displacements are were recorded at mid-point. All the beams failed between 5 kips and 9 kips. The design load, which is not plotted in the figure, is 20 kips. A significant discrepancy between the predicted and the experimental results is thus observed. Possible reasons for this discrepancy will be discussed in the following section.

All beams exhibited brittle failure without prominent display of ductility or yielding of steel. Little variation between tested beams of the same design can be observes. The slight variation is partially due to the fact that there are initial imperfections built into the manufacturing of the beams, such as a minor bent or cracking along the contour of the reinforcement, causing the beams to fail at undesirable loads or display diverging ductility behavior. Although the experimental results did not conform with the predicted results by the

36

algorithm, they are at least consistent among themselves. Fig.5-2-2 below displays some of the most characteristic failures.

(a) Beam with 75% volume
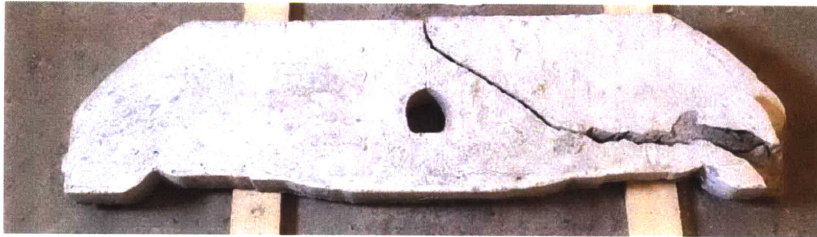
(b) Beam with 85% volume

(c) Beam with 90% volume

(d) Beam with 95% volume

(e) Beam with full volume and traditional reinforcement

(f) Beam with full volume and optimized reinforcement

Fig.5-2-2 Characteristic failures of the beams

It is surprising that none of the tested beams survived the design load. This discrepancy can possibly be caused by the lack of bonding between concrete and the reinforcement. From a close examination of the failure cracks among the beams, it is easily observable that the steel completely detaches from the concrete, leaving a polished surface between the two phases. Fig.5-2-3 displays the polished surface of contact along the longitudinal surface. It is extremely difficult to increase the surface roughness of the steel reinforcement in these surfaces. Although corrugation is added onto the top and bottom surface, the steel reinforcement still does not bond with the concrete well. Fig.5-2-4 displays the lack of bonding between the corrugation and the concrete. One possible mean to increase the bonding is by adding curvature and fillet to the corrugation, as done in Jackson's research [9] where the type of bonding failure between concrete and steel reinforcement was not observed to the same extent. Fig.5-2-4 (a) also displays a well-bonded region between the end anchor that contains circular fillet as oppose to other chamfers where only straight lines and angles are present.

Fig.5-2-3. Polished surface of contact between the steel and concrete

(a)

(b)
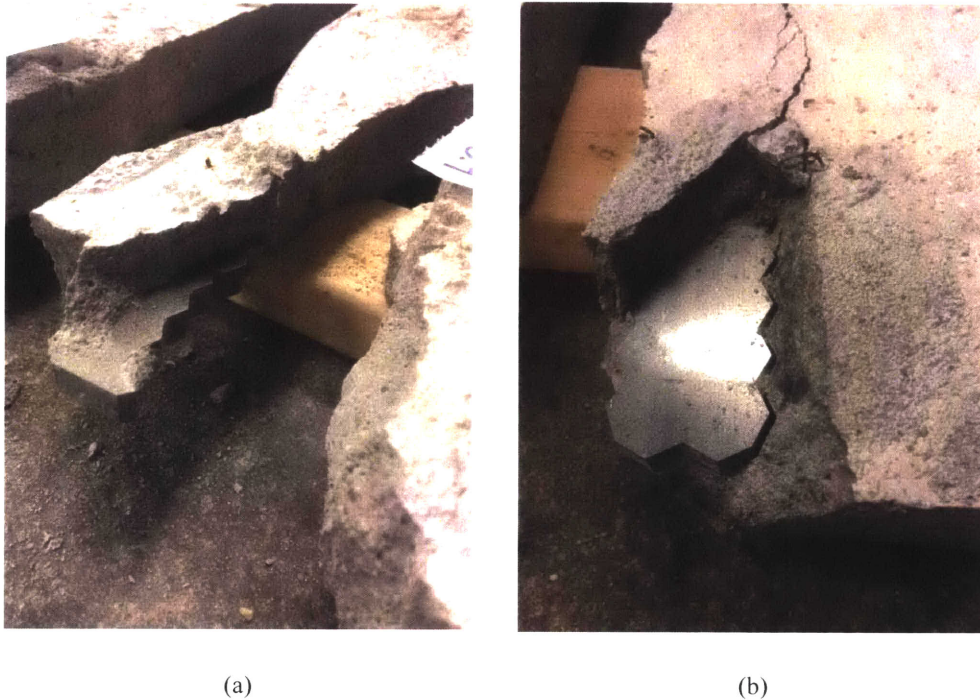
Fig.5-2-4 Lack of bonding between the corrugation and the concrete

Another possible reason for the reduction in strength is that the steel reinforcement is too thick and takes a quarter of the total width of the beam (thickness of the steel reinforcement = 0.5 in, width of the beam = 2 inches). Under the combined effect that the concrete does not bond well with the steel, the lack of concrete on both sides of the reinforcement significantly decreases the shear capacity of the beam. Future research can be conducted by using thinner steel plates for the reinforcement and adding curvature to the corrugation.

6. Discussion of Results

As outlined in the previous section, all tested beams exhibited premature failure; most likely caused by a poor bond between the reinforcement and concrete phase. However, since the failure mode was consistent over most all beams, a performance comparison can still be made. This section will offer four comparison which will be discussed in greater details in the following section.

I.   Comparison among the performance of the full concrete volume beams
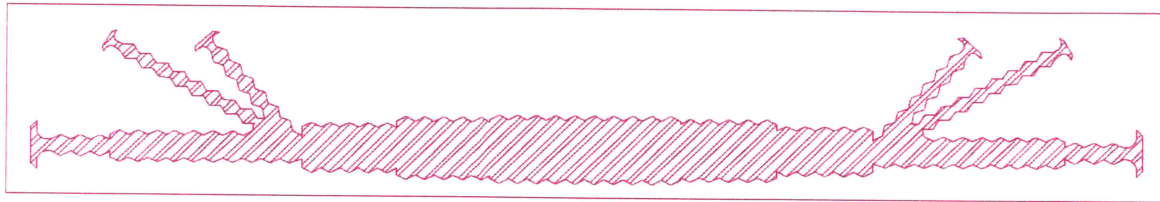
(a) Full volume beam with optimized reinforcement
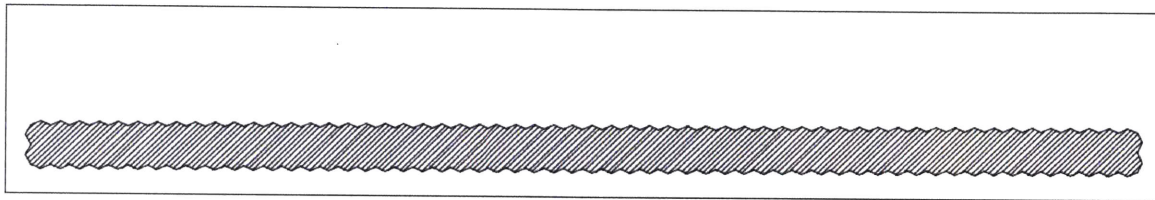
(b) Full volume beam with traditional reinforcement

Fig.6-3 Configuration of beams with full concrete volume
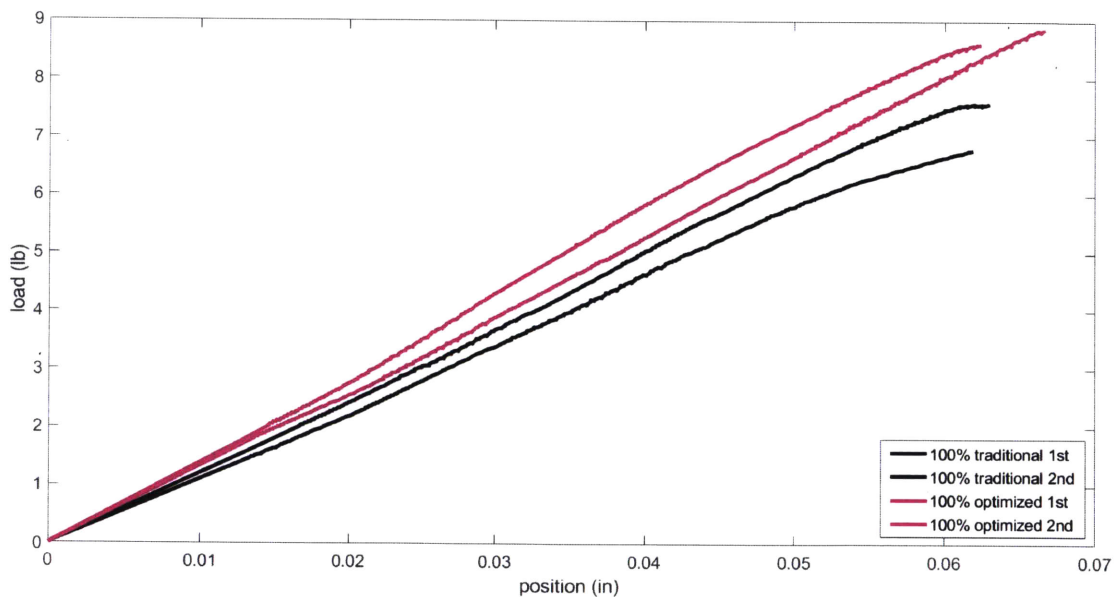
Fig.6-4 Load vs. displacement curves for the full concrete volume beams

40

Fig.6-4 displays the load vs. displacement curve experimentally obtained for the two beam types with 100% concrete volume. The pink curves detail the performance of the beams with the optimized steel layout obtained from the the 75% volume fraction design, with its configuration displayed in Fig.6-3 (a). The black curves detail the performance of the beams with traditional uniform reinforcement, with its configuration displayed in Fig.6-3 (b). Both types of beams use the same amount of steel reinforcement, the only difference being the layout, where one obtained through traditional analysis while the other is obtained with topology optimization. Their respective ultimate loads are displayed in Table 6-2.

| Full Volume		Max Load (lb)	Average	Percentage Increase
Traditional	1st	8864.33	8732.48	21.49%
	2nd	8600.64		
Optimized	1st	6787.38	7187.96	
	2nd	7588.54		

Table 6-2 Ultimate load for the full volume beams

As can be seen by Table 6-2, using topology-optimized steel reinforcement has increased the strength dramatically with an average of 21.5%. The absence of shear reinforcement in the beams with one traditional steel bar in the tension zone significantly limits the performance. The extra four steel bars from the optimized reinforcement provide transverse strength to the beams. As we can observe from Fig.5-2-2 (f) in the previous section, the shear cracks of the beams with optimized reinforcement follow the contour of the reinforcement, whereas all the beams with traditional reinforcement failed brittlely and locally around the supports. This demonstrates the critical need for transverse reinforcement that can be provided through the reinforcement suggested in the topology-optimized design. It also potentially suggests that by only optimizing the layout the reinforcement while maintaining the volume of reinforcement, engineers can arrive at even higher capacity designs.

41

II.   Comparison among the performance of the beams with partial concrete volumes
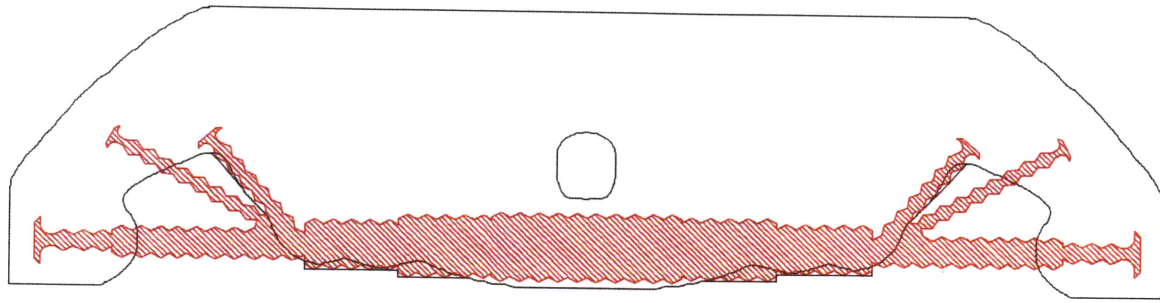
(a) 75% concrete volume
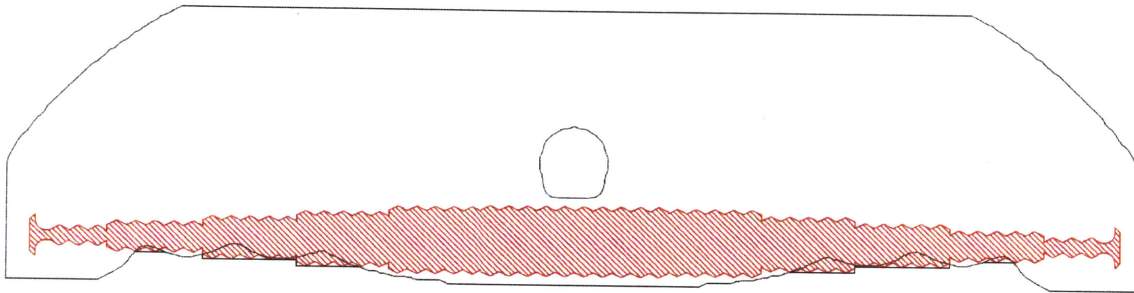
(b) 85% concrete volume
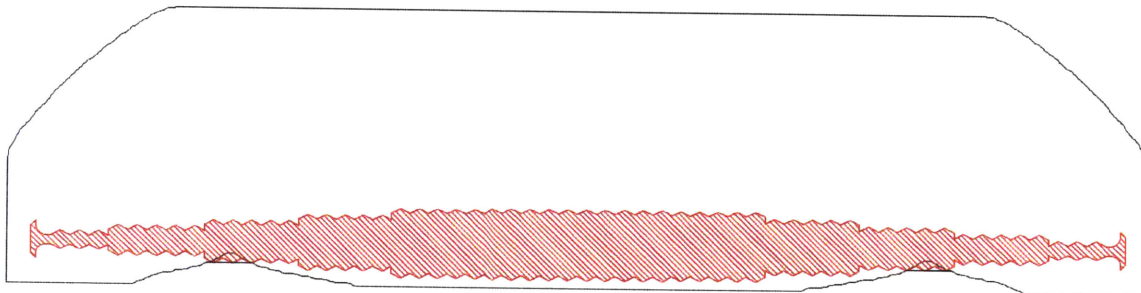
(c) 90% concrete volume
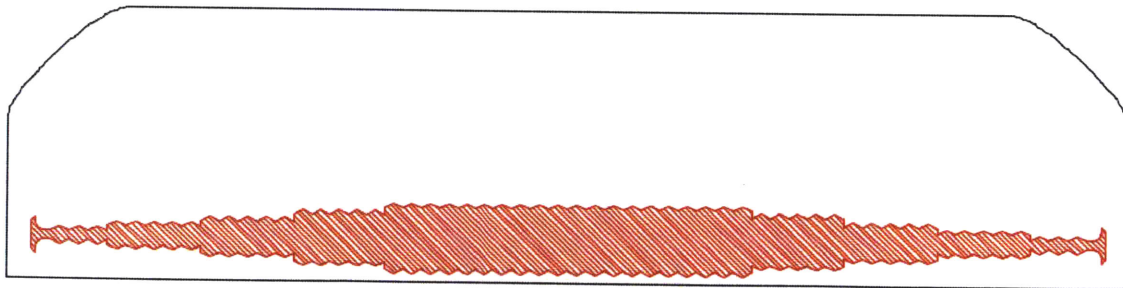
(d) 95% concrete volume

Fig.6-5 Configuration of beams with partial concrete volume
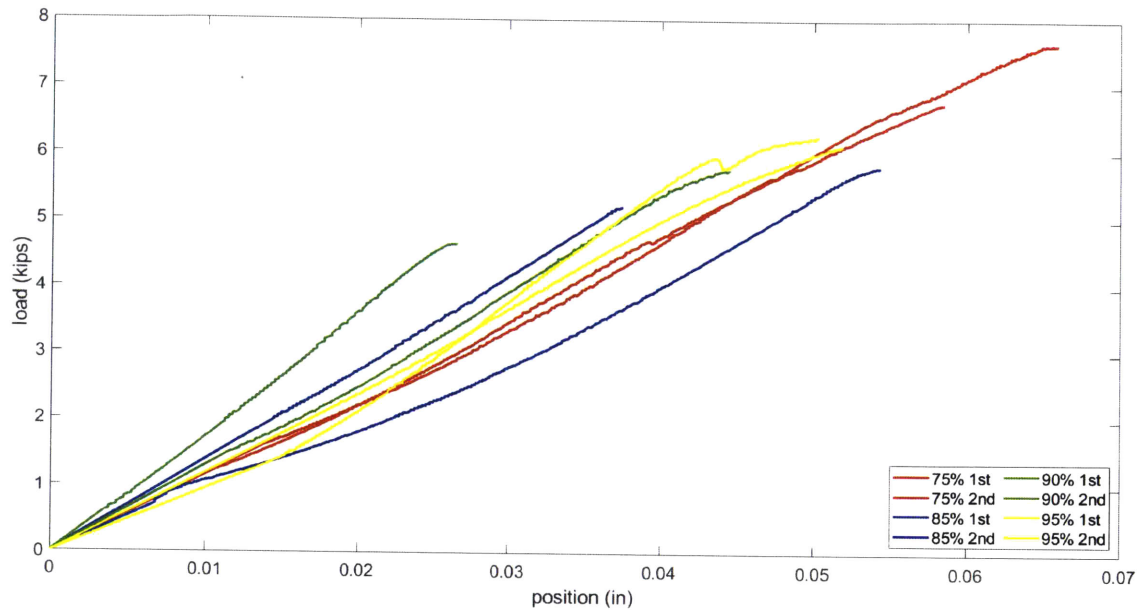
Fig.6-6 Load vs. displacement curves for the beams with partial volumes

Designing reinforced concrete beams using Strut-and-Tie Models will result in under-utilized areas where minimal force is predicted to present. Thus, the concrete volume within these regions does not contribute to the overall strength of the beam. Fig.6-6 displays the load vs. displacement curves for the beams with a portion of the under-utilized regions removed. As can be observed, the capacity of the beams gradually decreases when more volume extracted. Fig.6-5 displays the configurations of the beams including their reinforcement layout from 75% to 95% volume. Again, the volume of reinforcement among the beams is strictly kept equal. It is interesting that when the upper bound of the volume constraint is set, below a certain threshold the optimized layout of the reinforcement starts to alter as well. The difference in reinforcement patterns between the 75% volume beams and that of the rest of the partial volume beams is the primary reason for the difference in performance. It again demonstrates that the algorithm is not adequate in determine the optimized layout of the reinforcement when we retain most of the material.

III.   Comparison among the performance of all concrete volumes
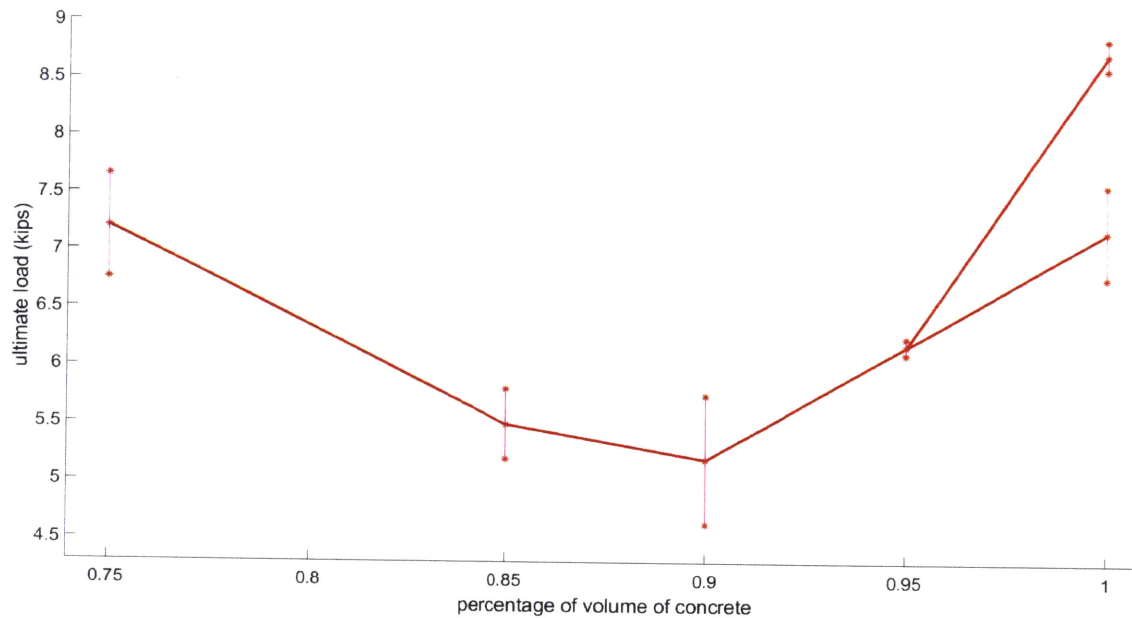
Fig.6-1 Ultimate load of experimentally tested beams as functions of their concrete volume

Fig.6-1 displays the ultimate loads for all the beams represented by '*' plotted against their concrete volume. The averages are computed and linked to show the overall trend of the capacities. Two sets of capacities for the beams with full concrete volume are displayed with the higher set being the ones with the optimized reinforcement. Their respective ultimate loads are displayed in Table 6-1:

Percentage Volume			Max Load (lb)	Average (lb)
100%				
Traditional		1st	6787.38	7187.96
		2nd	7588.54	
Optimized		1st	8864.33	8732.48
		2nd	8600.64	
75%		1st	7656.98	7205.35
		2nd	6753.72	
85%		1st	5196.29	5499.81
		2nd	5803.33	

90%	1st	5758.45	5197.97
	2nd	4637.50	
95%	1st	6260.01	6189.32
	2nd	6118.63	

Table 6-1 Ultimate load of experimentally tested beams

As seen in Table 6-1 and Fig.6-1, a local minimum seems to occur around 90% volume fraction. This is surprising since the reinforcement design of the beams with 90% concrete volume does not differ significantly from that of the beams with 85% concrete volume. However, the second test of the 90% concrete volume had notable cracks and initial bent prior to testing, which possibly could have resulted in lower-than-expected capacity. Fig.6-2 displays the initial cracking in the beam before testing.

Fig.6-2 Initial cracking in the beams

The beams with 95% volume fraction and optimized reinforcement have an average strength reduction of 29.1% comparing to the beams with full volume and optimized reinforcement, and the beams with 85% volume fraction have an average strength reduction of 37%. This tradeoff strongly disfavors material savings over strength, meaning with little material volume extracted incurs a significant strength reduction. This is indicative that the

45

topology optimization algorithm that uses Strut-and-Tie Model does not work satisfactorily for high concrete volumes. At high concrete volumes, the compressive force flow is no longer truss-like and the resulting reinforcement does not have sufficient shear capacity. However, the beams with 75% volume fraction and optimized reinforcement perform soundly. This suggests that future research should implement means to force the optimizer to create Strut-and-Tie-alike optimized reinforcement even for high concrete volumes.

IV.   Comparison among the performance of the full volume beams and 75% volume fraction
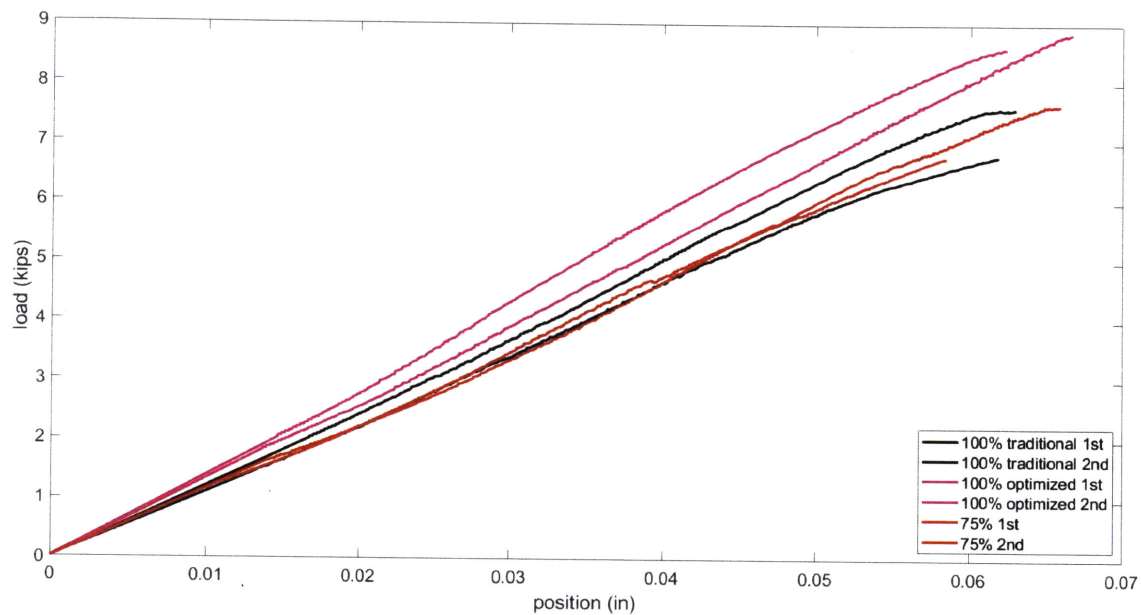
Fig.6-7 Load vs. displacement curves for the beams with 100% concrete and the topology-optimized beams with 75% concrete

Fig.6-7 displays the load vs. displacement curve for the beams with 100% concrete with two different layouts of the reinforcement as well as the topology-optimized beams with 75% concrete volume. The obtained ultimate loads are compared in Table 5.5.

			Max Load (lb)	Average	Percentage increase
100 % Volume					
	Traditional	1st	6787.38	7187.96	
		2nd	7588.54		
75% volume		1st	7656.98	7205.35	0.24%
		2nd	6753.72		

(a)

46

		Max Load (lb)	Average	Percentage increase
100 % Volume Optimized	1st	8864.33	8732.48	
	2nd	8600.64		
75% volume	1st	7656.98	7205.35	-17.49%
	2nd	6753.72		

(b)

Table 6-3 Ultimate load for the beams with 100% concrete and the topology-optimized beams with 75% concrete

As can be seen from Table 6-3 (a), the topology-optimized beams with 75% concrete behave almost identically to the beams with full volume and traditional reinforcement. Since both beams use the same amount of reinforcement, this demonstrates that the 25% reduction in concrete volume can be well supplemented with different and optimized reinforcement layout. Using topology optimization successfully maintains the capacity of the beams even with a significant reduction in material volume. However, the only beams that did not show clear signs of reinforcement slipping was that of the 75% concrete volume. It is therefore possible that the superior performance observed in the 75% volume beams is caused by proper bonding of the concrete and the reinforcement. Thus, it would be interesting to conduct further investigations in the future with a reinforcement type that possesses better bonding qualities.

As we can see from table 6-3 (b), the capacity of the beams with 75% concrete volume and optimized reinforcement is 17.5% lower compared to the beams with full volume and the same reinforcement. A 25% savings in concrete material volume incurs a 17.5% reduction in strength, which demonstrates that the algorithm is extracting volume from under-utilized areas within the beam. Further studies can be done by performing a finite element analysis on the full-volume beam and observe whether the under-utilized areas from the model coincide with the material reduction chosen by the algorithm.

7. Conclusion

This research has demonstrated that topology optimization can produce light-weight reinforced concrete beams with the same performance as traditional designs. The aim of this research was to experimentally investigate the consequences of removing underutilized concrete regions from topology-optimized RC beams. Five different concrete volumes, 75%, 85%, 90%, 95%, and full volume were chosen to investigate the relationship between the reduction of strength and the material savings.

The resulting geometries, purely driven by the algorithm combining both the concrete phase and the reinforcement phase, are novel. The experimental results show that the beams with 75% concrete volume outperform all other partial concrete volume beams. This can be due to the fact that the optimized steel reinforcements within the beams with 75% volume fraction increase the beams' shear capacity tremendously. Secondly, the beams with 75% concrete volume perform almost identically to the beams with full volume and traditionally-sized reinforcement. This demonstrates that the reduction in strength that is caused by material saving can be remedied by optimizing the layout of the steel reinforcement using topology optimization. For the case studies in this work, a 25% reduction of concrete volume was achieved while maintaining the same load capacity. Lastly, the beams with full volume fraction and topology-optimized steel reinforcement unsurprisingly have the best performance. This demonstrates that the strength of regular prismatic beam can be dramatically increased by having non-conventional optimized reinforcement.

The manufacturing process used in this work requires attention to detail and careful planning to prevent unanticipated failures. In this work, bonding failures between the concrete phase and the steel plates used as reinforcement was observed for most test specimens. To fully validate the trends observed in this work, future research that use more traditional reinforcement methods is recommended.

Reference

[1]

Forty, A. (2013). *Concrete and Culture: A Material History*. Reaktion Books.

[2]

Jipa, A., Bernhard, M., Meibodi, M., and Dillenburger, B. (2016). "3D-Printed Stay-in-Place Formwork for Topologically Optimized Concrete Slabs."

[3]

Bendsoe, M. P., and Sigmund, O. (2004). *Topology Optimization: Theory, Methods, and Applications*. Springer-Verlag, Berlin Heidelberg.

[4]

Darwin, D., Dolan, C., and Nilson, A. (2016). *Design of Concrete Structures*. McGraw Hill Education.

[5]

Gaynor Andrew T., Guest James K., and Moen Cristopher D. (2013). "Reinforced Concrete Force Visualization and Design Using Bilinear Truss-Continuum Topology Optimization." *Journal of Structural Engineering*, 139(4), 607–618.

[6]

Dombernowsky, P., and Søndergaard, A. (2012). "Design, Analysis and Realisation of Topology Optimized Concrete Structures." *Journal of the International Association for Shell and Spatial Structures*, 53, 209–216.

[7]

Liew, A., López, D. L., Van Mele, T., and Block, P. (2017). "Design, fabrication and testing of a prototype, thin-vaulted, unreinforced concrete floor." *Engineering Structures*, 137, 323–335.

[8]

Jewett, J. L., and Carstensen, J. V. (2019). "Topology-optimized design, construction and experimental evaluation of concrete beams." *Automation in Construction*, 102, 59–67.

[9]

Jewett, J., and Carstensen, J. V. (n.d.). "Experimental Investigation of Strut-and-Tie Layouts in Deep RC Beams Designed with Hybrid Bi-linear Topology Optimization."

[10]

Dapogny, C., Faure, A., Michailidis, G., Allaire, G., Couvelas, A., and Estevez, R. (2017).

"Geometric constraints for shape and topology optimization in architectural design." *Computational Mechanics*, 59(6), 933–965.

[11]

Frearson, A. (2013). "Qatar National Convention Centre by Arata Isozaki." *Dezeen*, <https://www.dezeen.com/2013/08/22/qatar-national-convention-centre-by-arata-isozaki/> (Apr. 18, 2019).

[12]

"100 Mount Street." (n.d.). *SOM*, <http://www.som.com/projects/100_mount_street> (Apr. 18, 2019).

[13]

Stromberg, L. L., Beghini, A., Baker, W. F., and Paulino, G. H. (2012). "Topology optimization for braced frames: Combining continuum and beam/column elements." *Engineering Structures*, 37, 106–124.

[14]

Bruggi, M. (2009). "Generating strut-and-tie patterns for reinforced concrete structures using topology optimization." *Computers & Structures*, 87(23), 1483–1495.

[15]

Liang, Q. Q., Xie, Y. M., and Steven, G. P. (2000). "Topology optimization of strut-and-tie models in reinforced concrete structures using an evolutionary procedure." *ACI Structural Journal*, 97, 322–330.

[16]

Victoria, M., Querin, O. M., and Martí, P. (2011). "Generation of strut-and-tie models by topology design using different material properties in tension and compression." *Structural and Multidisciplinary Optimization*, 44(2), 247–258.

[17]

Svanberg, K. (1987). "The method of moving asymptotes—a new method for structural optimization." *International Journal for Numerical Methods in Engineering*, 24(2), 359–373

[18]

ACI Committee 318. (2014). "318-14: Building Code Requirements for Structural Concrete and Commentary."

[19]

"McMaster-Carr." (n.d.). <https://www.mcmaster.com/> (May 8, 2019).

[20]

Bendsøe, M. P., and Sigmund, O. (1999). "Material interpolation schemes in topology optimization." *Archive of Applied Mechanics*, 69(9), 635–654.

[21]

Guest, J. K., Prévost, J. H., and Belytschko, T. (2004). "Achieving minimum length scale in topology optimization using nodal design variables and projection functions." *International Journal for Numerical Methods in Engineering*, 61(2), 238–254.

[22]

Bendsoe, M. P., and Sigmund, O. (2004). *Topology Optimization: Theory, Methods, and Applications*. Springer-Verlag, Berlin Heidelberg.

[23]

"Rhino 6 for Windows." (n.d.). <https://www.rhino3d.com/> (May 9, 2019).

[24]

Claisse, P. (2016). *Civil Engineering Materials - 1st Edition*. Butterworth-Heinemann.